Final Master Dissertation

Nanostructured Materials for Nanotechnological Applications

Dye-sensitized titanium dioxide anode for Photoelectrochemical water splitting

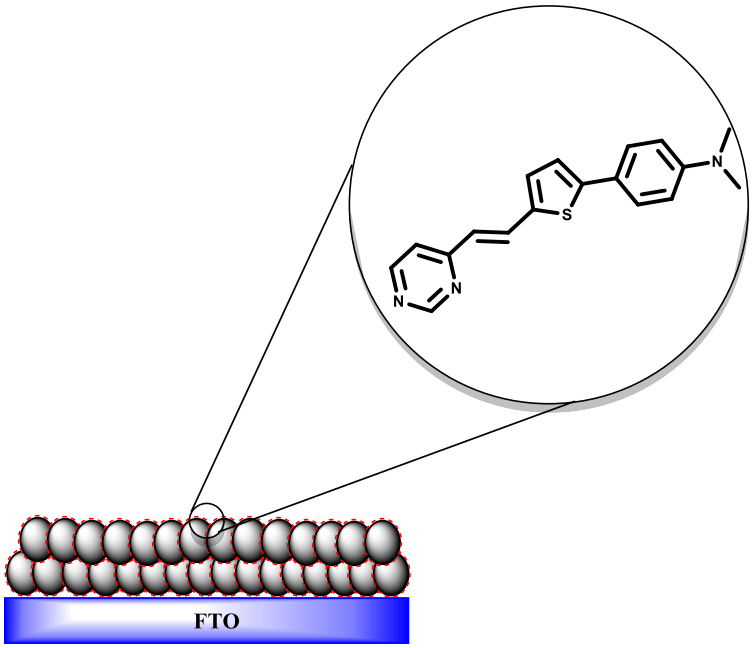

Author: **Sergio Angoy Benabarre**

Supervisors: **Alejandro Ansón Casaos**

María Jesús Blesa Moreno

Universidad Zaragoza 1542

CSIC Consejo Superior de Investigaciones Científicas

icb Instituto de Carboquimica

INMA Instituto de Nanociencia y Materiales de Aragón

Acronyms

rGO: Reduced Graphene Oxide

DSSC: Dye-Sensitized Solar Cell

UV: Ultraviolet

PSII: Photosystem II

PSI: Photosystem I

P_{680}: Chlorophyll

P_{680}^{+}: Excited chlorophyll

$Pheo_A$: Pheophytin

Q_A: Plastoquinone

Y_Z: Tyrosine

PEC: Photoelectrochemical cell

CIGS: Copper Indium Gallium Selenide

PV-electrolyzer: Photovoltaic Electrolyser

FTO: Fluorine-doped Tin Oxide

THF: Tetrahydrofuran

s: Singlet

d: Doublet

m: Multiplet

J: Coupling constant

FTIR: Fourier Transform Infrared

^{1}H-NMR: Proton Nuclear Magnetic Resonance

^{13}C-NMR: Carbon-13 Nuclear Magnetic Resonance

HRMS: High Resolution Mass Spectroscopy

ESI: Electrospray Ionization

GO: Graphene Oxide

ATR: Attenuated Total Reflection

SEM: Scanning Electron Microscopy

FT-IR: Fourier Transform Infrared

ITC: Intramolecular Charge Transfer

DPV: Differential Pulse Voltammetry

NHE: Normal Hydrogen Electrode

CV: Cyclic voltammetry

MS: Mass spectrometry

Std. dev.: Standard deviation

η: Efficiency

V_{oc}: Open-circuit voltage

J_{sc}: Short-circuit current density

FF: Fill Factor

Table of contents

Abstract

This work is focused on the development of a promising device that can perform the water splitting reaction using sunlight. The photoanode developed is inspired by the DSSCs with dye-sensitized TiO_2 as the base structure. Besides checking the potential of the TiO_2/dye system for the oxidation of water, we have applied some variations in the device with the aim of improving its characteristics. The modifications made are, in one hand, the application of several reduction cycles before the measurements and, on the other hand, the addition of rGO layers with different thicknesses. The project is divided in several parts, it starts with the synthesis of the dye used, AT-Piri, together with the optimization of the immersion time; next, the characterization of photoanodes and its photochemical study; finishing with the measurement of the photovoltaic parameters of DSSC-type cells built in the laboratory.

Resumen

Este trabajo está enfocado en el desarrollo de un dispositivo prometedor que pueda llevar a cabo la división del agua usando la luz del sol. El fotoánodo está inspirado en las DSSC con TiO_2 sensibilizado por colorante. Además de comprobar el potencial del sistema TiO_2/dye para la oxidación del agua, hemos aplicado algunas variaciones en el dispositivo con el objetivo de mejorar sus características. Las modificaciones realizadas son, por un lado, la aplicación de varios ciclos de reducción antes de las mediciones y, por otro lado, la adición de rGO con diferentes espesores para comprobar su influencia. El proyecto está divido en diferentes partes: comienza con la síntesis del colorante, AT-Piri, junto con la optimización del tiempo de inmersión; seguido por la caracterización de los fotoánodos y su estudio fotoquímico; terminando con la medida de los parámetros fotovoltaicos de celdas solares tipo DSSC construidas en el laboratorio.

1. Introduction

In recent years, the negative environmental consequences arising from the fast economic development and the growth of world population have been increasing and, in particular, the consequences derived from pollution are becoming alarming. One of the side-effects is the increase in the concentration of carbon dioxide in the atmosphere by the combustion of fossil fuels and emissions of greenhouse gases. Concern for the preservation of the environment, together with the growing global energy demand, make the search for sustainable carbon-free energy alternatives one of the fields of strategic research at present. For this reason, the systematic and deep decarbonisation of the energy system is the political horizon priority to be achieved in the twenty-first century.

At this respect, the water splitting represents a promising alternative to substitute the carbon-based energies. In this reaction, we seek to take advantage of solar energy as an inexhaustible energy source to oxidize water, generating molecular oxygen and protons, which will be reduced in a later stage to hydrogen. The hydrogen produced is accumulated for a later use as a fuel, allowing the storage of solar energy in the form of chemical energy. Both oxygen release and hydrogen combustion are clean processes that do not involve any kind of pollution, being consistent with the principles of green chemistry. The development of this alternative was inspired by plant photosynthesis, in which plant organisms use solar energy to synthesize nutrients.

Taking into account this scenario, the device proposed is an anode based on dye-sensitized titanium dioxide. The TiO_2 is an excellent semiconductor which has the drawback of absorbing light only in the UV-range, being inadequate for the application exposed. Hence, the dye sensitization perfectly matches to develop a device with promising properties to perform the oxidation of water. Since the dye absorbs light in the visible range, it extends the range in which the device can take advantage of the sunlight to produce de desired hydrogen.

1.1. Photosynthesis as inspiration for water splitting

With the aim of further understanding how the water splitting works, it will be instructive to explain briefly the process in which it is inspired, the photosynthesis. The

interesting part for us is the one that occur in the photosystem II (PSII), where the photolysis of water happens by solar energy.

Natural photosynthesis takes place in the membranes of the thylakoids, which are located in the chloroplasts. The process begins when the sunlight is absorbed by the chlorophyll, providing energy to oxidize water in PSII. Oxygen is produced as a secondary product together with protons and electrons. The electrons are combined with CO_2 in the photosystem I (PSI) following the Calvin Cycle, forming carbohydrates. Ultimately, the photosynthetic organisms store the sunlight as chemical energy through the photosynthesis.

The balance of the reactions that occur in the PSII is:

$$2H_2O + 2NADP^+ + 3ADP + 3Pi + 8h\upsilon \rightarrow O_2 + 2NADPH + 2H^+ + 3ATP \qquad \text{(eq. 1)}$$

The mechanism, see **Figure 1a**, starts when the sunlight induces the charge separation between chlorophyll (P_{680}) and pheophytin ($Pheo_A$), followed by an interchange of electrons to a plastoquinone (Q_A). Biologically, the water oxidation is catalysed by the cluster Mn_4CaO_5, **Figure 1b**. The cluster is progressively oxidized by a Tyrosine (Y_z), which transfers one electron between the cluster and the P_{680}^+. The P_{680} is then restored, ready for another cycle of the mechanism. After 4 cycles, the cluster has accumulated enough potential to oxidize water, restored for another catalytic cycle[1].

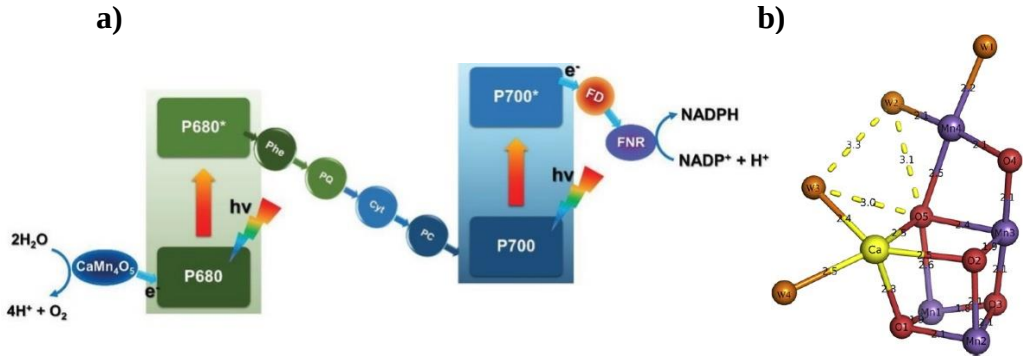

Figure 1. **a)** Part of the photosynthetic mechanism[2]. **b)** Mn_4CaO_5 cluster[1].

The major disadvantage of the technologies that use the sunlight is the incapacity to store the energy produced, as them convert it directly in electricity. This problem can be solved with the artificial photosynthesis, producing hydrogen that can be stored for a later use[3].

In the natural process the electrons are used to reduce different nucleotides. Its purpose in the artificial approach is to reduce protons, forming molecular hydrogen that will serve as fuel. Hence, an artificial photosynthetic system links the oxidation of water to produce electrons that will lead on the production of hydrogen. The reactions that happen are:

$$2H_2O \rightarrow O_2 + 4H^+ + 4e^- \quad \text{(eq. 2a)}$$

$$4H^+ + 4e^- \rightarrow 2H_2 \quad \text{(eq. 2b)}$$

As it was mentioned, the devices designed with this purpose must have, at least, a light harvesting substance, a catalyst to facilitate the redox reactions, an electrolyte for the ion transport and a membrane between the cathode and the anode to ensure the charge separation and storage of products. Three different cells can be used (**Figure 2**): a PV-electrolyzer which is efficient, but expensive; the photocatalytic mixed colloids that are not expensive but do not let to store the products individually; and the integrated PECs, a mix of the previous combining the efficiency of the first and the simplicity of the second. Ideally, the last one represents the most promising alternative.

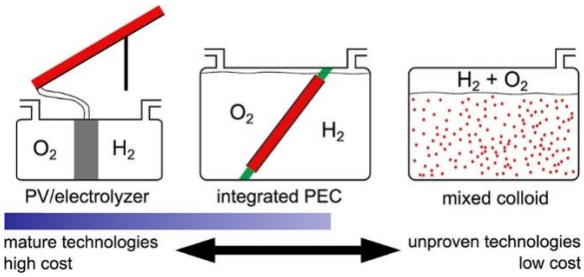

Figure 2. Different types of cells for water splitting[4].

1.2. Integrated PECs

The integrated PECs represent an interesting concept to perform the water splitting reaction directly induced by sunlight. These cells have three main parts[5]: the photoanode (with a water splitting catalyst and a n-type semiconductor), the photocathode (with a catalyst for hydrogen reduction and a p-type semiconductor) and a membrane (**Figure 3**). It is worthy to explain the steps that happen in each reaction cycle to understand the function of each constituent.

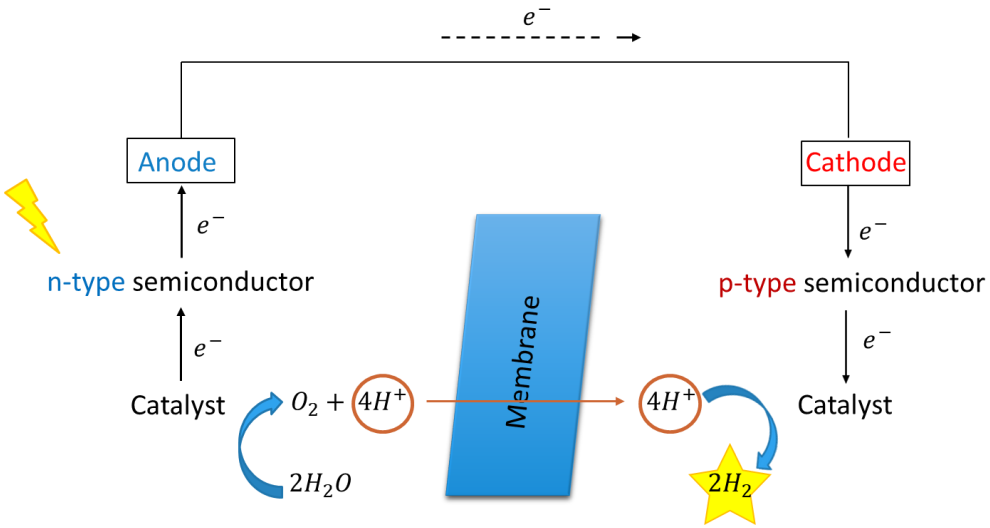

Figure 3. Diagram of an integrated PEC.

The process begins when the absorption of a photon by the n-type semiconductor generates an electron-hole pair and thus an electronic vacancy in its surface. The n-type semiconductors may be doped with elements that provide free electrons, facilitating the formation of "holes". The vacancy is filled by transferring one electron from the electrolyte. After repeating the process 4 times, the catalyst oxidize water to O_2. Moreover, the electrons removed from the anode are transported by the external wire to the cathode, where they pass to the p-type semiconductor material. The p-type semiconductors are doped with elements that generate electronic vacancies, serving as charge carriers in the electrode. Examples of this type of materials are CdTe or CIGS. Finally, the electrons reach the catalyst, concluding in the formation of hydrogen. The membrane has a double function, on the one hand, it allows to obtain separately the products formed in each compartment, oxygen in the anode and hydrogen in the cathode, in addition it is permeable to the pass of protons, formed from water, for its reduction in the cathode.

1.3. Artificial water splitting

The first method developed for the photocatalytic decomposition of water was published by Fujishima and Honda in 1972[6]. It was performed using a photoelectrochemical cell with TiO_2 as the anode and platinum as the cathode. Since then, the use of TiO_2 nanomaterials for this and other applications have been extensively studied. Its popularity over other similar photocatalysts is due to its strong

oxidizing capabilities, superhydrophilicity under UV-light radiation, chemical stability, nontoxicity, durability and low cost[7].

The major drawback of the TiO_2 is its high band gap (3.2 eV)[8] which makes it active only under UV-light. It means that only the 3-5% of the light provided by the sun can be used[9]. Considering that the aim of this process is to take advantage of the sunlight, it is required that the material utilizes the sun radiation as possible. At this respect several approaches have been developed such as doped-TiO_2 with different metal ions[10] (Fe or Rd) or with nonmetal ions[11] (N and S). Other strategy followed is dye sensitization[12, 13], the one in which this project is focused on.

Since Grätzel and O'Regan developed the first dye-sensitized solar cell in 1991[14], the interest in this strategy to harvest visible-light has been growing. This success is due to its low cost and efficiencies. Following a similar approach in terms of structure and mechanism, the main part of the cell, the dye sensitized TiO_2, has been studied as anode for the photoelectrochemical water splitting. Despite the wide used of ruthenium-based dyes[15], the fully organic sensitizers represent a more viable alternative as their cost is considerably lower. The structure of this kind of dyes often consists in three main parts: a donor group, a π-conjugated bridge and an acceptor group (D-π-A). The dye is anchored to the TiO_2 through the acceptor group, which should have a good electronic overlapping with the titania to facilitate the electron injection. The π-linker helps the electronic transport through the molecule. The source of electrons is the donor group, which is rich in electrons and starts the flow of charges with its photoexcitation[16]. The mechanism in this type of photoanodes follows a basic principle. When the dye is photoexcited, the electrons pass across the molecule and end injected in the conduction band of the titania. The electrons are used in the reduction of water to produce H_2 and the oxidized dye is regenerated upon the oxidation of the water[17]. A Scheme of this process is presented in **Figure 4**.

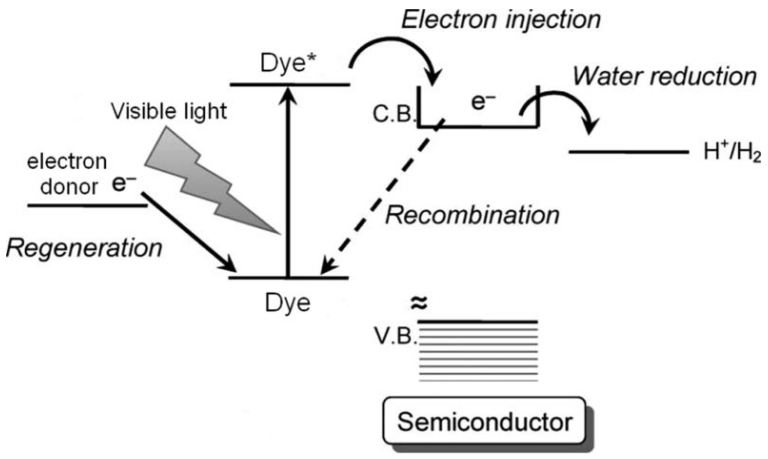

Figure 4. Water splitting mechanism in dye sensitized TiO_2[18].

In general, conventional dyes for DSSCs have been designed having a cyanoacetic group as anchoring and accepting group. The cyano group has strong electron withdrawing properties and the carboxylic group is the one that binds the dye to TiO_2[12]. However, a drawback of this chemical structure is that the ester bonds formed between TiO_2 and the carboxylic anchoring groups are easily hydrolyzed in aqueous environment, especially under alkaline conditions[19]. Such defects unavoidably lead to partial desorption of some dye molecules, which limits the durability of the photocatalyst to a certain extent. As an alternative approach, photosensitizers based on pyridine groups have been investigated and applied in photocatalytic water splitting systems[20, 21, 22]. It was found that the sensitizers with pyridyl anchors had better chemical adsorption stability on TiO_2 surfaces compared to the common carboxylate and phosphonate ones[23]. Therefore, the dye designed for these studies was a typical D-π-A system with aniline as donor, thiophene as π-spacer and pyrimidine acceptor and anchoring group (**Scheme 1**).

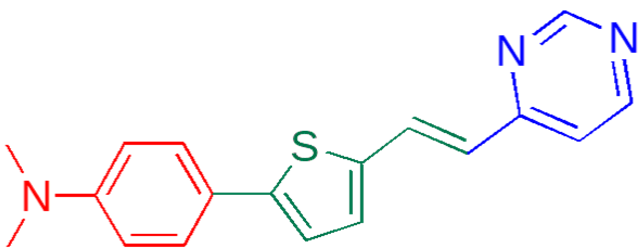

Scheme 1. D-π-A structure of dye

2. Objectives

The aim of this project is the development of a novel anode with adequate properties for the photoelectrochemical production of green hydrogen.

To reach this goal it is proposed to sensitize TiO_2 with an organic dye to merge the main properties of both components: the electrochemical catalytic activity of TiO_2 and the capability of taking advantage of a wide wavelength range of sunlight provided by the organic dye. Thus, the influence of an electrochemical reduction in the system or the addition of different rGO thicknesses will be explored.

Furthermore, the photoanode will be tested in a DSSC to check its performance.

3. Experimental

3.1. Chemicals and materials

The materials and installations used during the execution of this project were provided by the Carbon Chemistry Institute (ICB) and the Organic Chemistry Department of the University of Zaragoza. The chemicals used were acquired in Sigma-Aldrich. The TiO_2 and the Platinum paste were provided by GreatCell Solar and Dyesol, respectively. Two types of FTO were used, ones for DSSCs (15 Ω/sq sheet resistance) bought in Solaronix, and others for the photoanodes (70Ω/sq sheet resistance) supplied by Solems S.A. The graphene oxide used was from Graphenea.

3.2. Synthesis of AT-Piri

5-(4-(dimethylamino)phenyl)thiophene-2-carbaldehyde

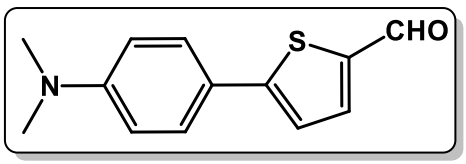

p-bromo-*N*,*N*-dimethylaniline (0.5g, 2.5 mmol) was dissolved in 10 mL of THF anhydrous at -78 ºC in a two-necked flask, under inert atmosphere (3 cycles vacuum-argon). Then, *n*-BuLi (1.69 mL, 4.1 mmol) was added, drop by drop. After 30 minutes, the reaction was cooled to ambient temperature. Subsequently, tributyltin chloride (0.9 mL, 3.0 mmol) was added, stirring the solution for 150 minutes. After that time, the reaction was stopped by adding 100mL of diethyl ether. The resulting organic phase were extracted, washed with a saturated solution of NaCl and water, dried with magnesium sulfate anhydrous, filtered, and finally, the solvent was removed with a rotary evaporator. The oily product was used, without purification, in the next step of the reaction.

The oily crude was dissolved in 15 ml of toluene anhydrous. After the addition of 5-bromo-2-thiophenecarboxaldehyde (0.19 mL, 1.5 mmol), the reaction was degasified with Argon for 15 minutes under stirring. Subsequently, $Pd(PPh_3)_4$ (0.15 g, 0.13 mmol) was added and the mixture refluxed at 115 ºC for 20 hours under stirring. The reaction was stopped by the addition of 50 mL of H_2O. The mixture was extracted with toluene (2x60 mL). The organic phase was washed with a saturated solution of NH_4Cl (1x60mL) and H_2O (2x60ml), dried with anhydride $MgSO_4$, filtered and the solvent was removed under reduced pressure. The crude product (1.64 g) was purified by flash chromatography increasing the polarity of the eluent from 85:15 to 75:25 to obtain the desired product. The purified product was washed with cold pentane, obtaining a yellow solid (255.75 mg, 44 %).

Molecular weight (g/mol): 231.31 **FTIR** (KBr) (cm^{-1}): 1643 (C=O) **Melting point** (ºC): 195 **^{1}H-NMR** (400 MHz, $CDCl_3$) δ (ppm): 3.02 (s, 6H), 6,72 (d, *J* = 8.8 Hz, 2H), 7.24 (d, *J* = 3.8 Hz, 1H), 7.57 (d, *J* = 8.8 Hz, 2H), 7.68 (d, *J* = 3.8 Hz, 1H), 9.82 (s, 1H) **^{13}C-NMR** (100 MHz, $CDCl_3$) δ (ppm): 40.2, 112.1, 120.9, 121.5, 127.5, 138.0, 151.2, 156.2, 182.4 **HRMS** $(ESI)^+$: calculated for $[C_{13}H_{13}NNaOS]^+$: 254.0610, found: 254.0607 $[M+Na]^+$.

<u>*N, N*-dimethyl-4-(5-((*E*)-2-(pyrimidin-4-yl)vinyl)thiophen-2-yl)benzamine</u>

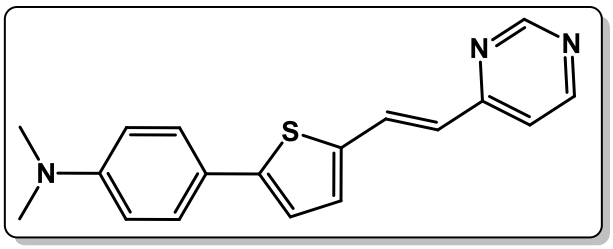

A stirred mixture of 5-(4-(dimethylamino)phenyl)thiophene-2-carbaldehyde (100 mg, 0.43 mmol) and 4-methylpyrimidine (40.5 µL, 0.43 mmol) in 5.9 mL NaOH (ac., 5M) was refluxed and Aliquat 336 was added (20 µL, 0.043 mmol). After 1 h, the mixture was cooled and the precipitate was filtered off and washed with water and the aqueous phase was extracted with CH_2Cl_2 (3x20 mL). The organic phase was dried with $MgSO_4$ and the solvent was removed under reduced pressure. The crude product was purified by flash chromatography increasing the polarity of the eluent hexane/ethyl acetate from 8:2 to 6:4 to obtain the desired product, an orange solid (29.4 mg, 22%).

M**olecular weight** (g/mol): 307.41 **FTIR** (KBr) (cm^{-1}): 1571 (C=N)**Melting point** (ºC): 227.7 **^{1}H-NMR** (400 MHz, $CDCl_3$) δ (ppm): 3.01 (s, 6H), 6.72 (d, *J*= 8Hz, 2H), 6.79 (d, *J*=16Hz, 1H),7.11 (d, *J* = 4 Hz, 1H), 7.18 (d, *J* = 4 Hz, 1H), 7.19 (s, 1H),7.52 (d, *J* = 8

Hz, 2H), 8.01 (d, *J* = 16 Hz, 1H), 8.62 (bs, 1H), 9.11 (s, 1H) **^{13}C-NMR** (100 MHz, $CDCl_3$) δ (ppm): 40.5, 112.5, 118.6, 119.9, 121.7, 123.0, 127.1, 130.8, 131.8, 150.6, 150.8, 157.3, 162.3**HRMS** $(ESI)^+$: calculated for $[C_{18}H_{17}N_3NaS]^+$: 330.1035, found: 330.1032 $[M+Na]^+$.

3.3. TiO_2 deposition and sensibilization

Initially, the strips can be covered by undesired substances such as dust or debris in general. Making the deposition on the surface at this moment would not be worthwhile due to lack of adhesion and to a decrease in the conductivity. Therefore, a cleaning process is required. The procedure starts by cleaning the FTO coated glass substrates using three different solutions: Mili-Q water with Hellmex III, Mili-Q water and ethanol. A glass holder was used to immerse de substrates in the solutions. All the cleaning steps had duration of 15 minutes under sonication. Then, the substrates were heated following a 4-hour program (with air and heated 30 minutes at 500˚C), after which they were placed in an ozonizer for 25 minutes. Once the cleaning process is done, the deposition of the TiO_2 paste (GreatCell Solar, 18 NR-AO) was made by screen printing. The paste was sintered in an oven following a 4.5-hour program (5 minutes at 325˚C, 5 minutes at 375˚C, 5 minutes at 450˚C and 15 minutes at 500˚C). The surface deposited was 1 cm x 1cm and the amount of paste was 0.6 mg/cm^2.The width of the TiO_2 layer was measured using a profilometer, giving a value of 4 μm.

The sensitization of the TiO_2 was made by using the final product described in 3.2. Before the exposition of the substrate to the dye, the TiO_2 had to be activated following the 4-hour heating program previously described to. Subsequently, the substrates were immersed in a 0.1 mM dichloromethane solution of the dye, AT-Piri, for 72 hours in darkness. After that time, the substrates were cleaned with dichloromethane and dried with a N_2 flow.

3.4. GO deposition

The deposition of the GO was automatized with the use of a "ND-SP Ultrasonic Spray Coater" from Nadetech Innovations (**Figure 5**). A solution of 0.5 mg/mL of GO in water was used as spraying solution. The substrates were placed in a hotplate at 140 ºC, the flow rate used was 20 mL/h and the nozzle distance was 60 mm. The number of layers varied from 20 to 40, depending on the sample. To ensure the drying of the layer

deposited, the substrates were placed in a hotplate at 140 ºC for 30 minutes. Later, the GO deposited was transformed to rGO by an electrochemical reduction process.

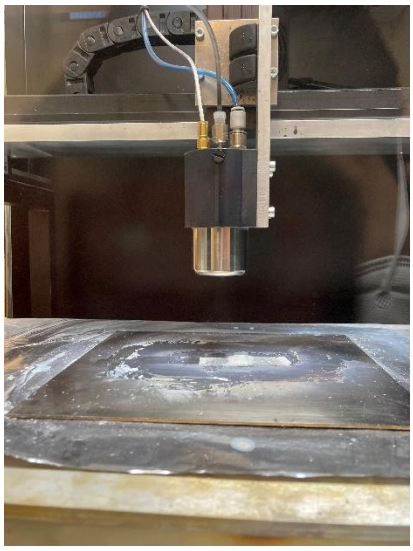

Figure 5. Spray coater used in the deposition of GO.

3.5. Photoelectrochemical experiments

The photoelectrochemical experiments were performed using an Autolab PGSTAT302 from MetroOhm. As light source we used a Xenon lamp of 150 W from LOT-Oriel, the power used during the experiments was approximately two suns (200 mW/cm^2). A system of three electrodes in a photoelectrochemical cell was used (**Figure 6**). The cell consists in a glass container with a quartz window through which the light passes. The three electrodes were an Ag/AgCl electrode as reference, a graphite bar as counter electrode and the electrode under study. A 0.1 M Na_2SO_4 solution was employed as electrolyte in all the cases. The cyclic voltametric experiments were performed in a range of -1.4 – 0.4 V in either illumination or darkness conditions, depending on the experiment. The potentiostatic experiments were performed under intermittent illumination at a constant voltage of 0 V (vs. Ag/AgCl).

Figure 6. Equipment used in the photoelectrochemical experiments.

3.6. Characterization techniques

Several characterization techniques were used during the project. The *UV-visible* was recorded with an UV-Vis Cary 6000 using either dye solution (CH_2Cl_2 as solvent) with different concentrations and films at different immersion times. *Raman* spectra were obtained by means of a HORIBA Jobin Yvon Raman spectrometer HR 800UV, using a 532 nm laser. *Scanning electron microscopy (SEM)* was performed in a SEM-EDX Hitachi S-3400 N. *Attenuated Total Reflection Infrared (ATR-FT)* spectra were recorded on a Perkin-Elmer Spectrum 100 FT-IR spectrometer (ATR range 250-4000 cm^{-1}). The *DPV* measurements were performed with a η-Autolab type III potentiostat using a glassy carbon as working electrode, Pt as counter electrode, Ag/AgCl as reference electrode, CH_2Cl_2 as solvent and Bu_4NPF_6 (0.1 $mol \cdot L^{-1}$) as supporting electrode.

4. Results and discussion

4.1. Organic dye

4.1.1. Synthesis of AT-Piri

The project started with the synthesis of the dye, the sensitive part of the anode. The reaction path to synthesize AT-Piri begins with the synthesis of the aldehyde precursor 1, previously published by Raposo[24] et al. The reaction starts by forming an organotin intermediate from *p*-bromo-*N*,*N*-dimethylaniline. This intermediate is then subjected to a Stille coupling, a reaction to form C-C bonds between the corresponding organotin and a halogen catalyzed by Pd (0). The resulting product of this coupling is the desired aldehyde precursor 1 (**Scheme 2**).

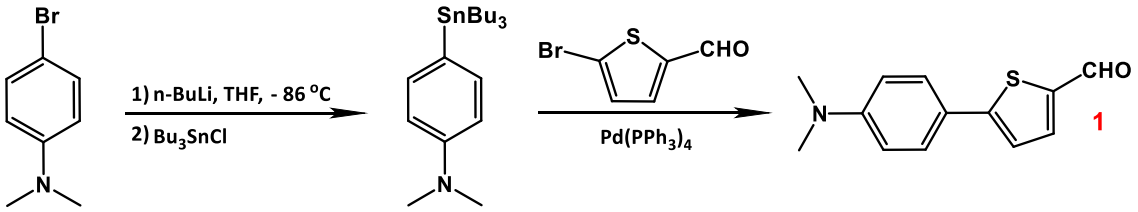

Scheme 2. Synthesis of the aldehyde precursor 1.

The synthesis follows with the reaction of the compound 1, in basic medium, with 4-methylpyrimidine. This is a condensation reaction catalyzed by Aliquat 336. The resulting product is AT-Piri (**Scheme 3**), which is the dye that will be used to sensitize the anode.

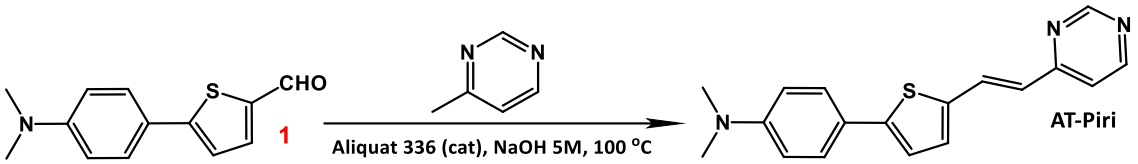

Scheme 3. Synthesis of AT-Piri

The corresponding FTIR, NMR and MS characterization of these compounds are depicted in the Appendix (**Figure A1-A9**).

4.1.2. Optical properties of AT-Piri

The optical properties of the dye were followed using different techniques. Initially, we have made a study of the dye in solution at different concentrations, **Figure 7a**. The spectrum shows a high energy band in the visible region (350–500 nm) which can be attributed to the intramolecular charge transfer (ICT) that occurs between the electron-withdrawing and electron-donating parts of the dye. This band suffers an hypsochromic shift on the film spectra with respect to the one in solution (**Figure 7b**), which can be attributed to the adsorption of the dye to the film[25].

a) **b)**

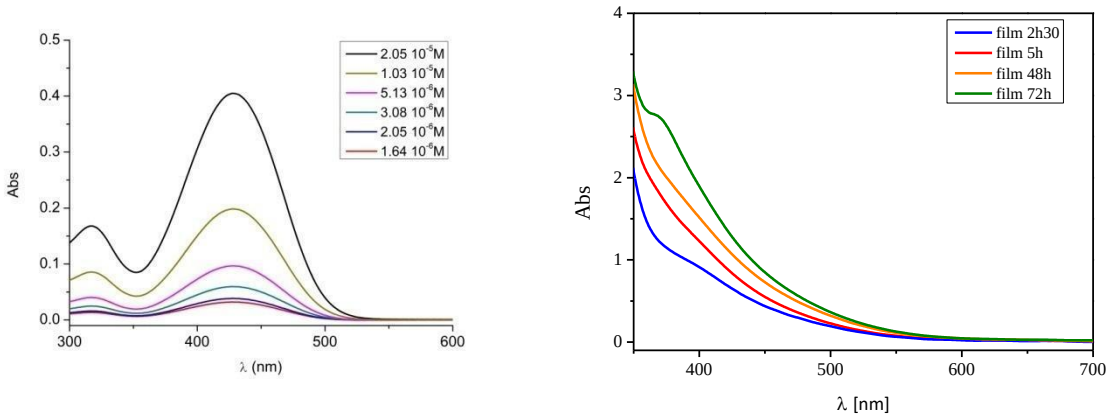

Figure 7. **a)** UV-vis absorption spectra in CH_2Cl_2. Concentration dependence of AT-Piri. **b)** UV-Visible study of TiO_2/AT-Piri films at different immersion times.

A key part in the development of the anodes is the sensitization of the TiO_2 paste with the dye. Hence, optimizing the immersion time is essential in order to improve the properties of our systems. For this reason, we have made a study in which we compare the amount of light absorbed by the system TiO_2/AT-Piri prepared with different immersion times (**Figure 7b**). In general, the ideal time can be assessed by choosing the one with the highest absorption rate, as it will make a better use of the sunlight by interacting with more photons. According to it, we have chosen an immersion time of 72 hours to sensitize our anodes since it absorbs more light than the others tested.

Table 1 summarizes the optical properties of AT-Piri measured by UV-visible and the potential values from a DPV measurements (**Figure A10**). Both the oxidation potential of ground and excited states can be used to assess if our dye is able to work as sensitizer in a DSSCs. On the one hand, the E^*_{ox} value is more negative than the conduction band of the TiO_2 (-0.50 V vs NHE), ensuring the injection of the electrons from the dye to the titania. On the other hand, the E_{ox} value (0.88 V) is higher than the redox potential of the I^-/I_3^- (0.40 V vs NHE), enabling the regeneration of the dye. Hence, AT-Piri is an adequate dye to work with.

Table 1. Optical parameters, transition energy $E_{0\text{-}0}$ and potential values E_{ox} and E^*_{ox}. The oxidation potentials were converted to NHE by addition of 0.199 V.

Dye	λ_{abs}[a] (nm)	λ_{cut} (nm)	ε [a] (10^4 $M^{-1}\cdot cm^{-1}$)	$E_{0\text{-}0}$[b] (eV)	E_{ox}[c] (V)	E^*_{ox}[d] (V)
AT-Piri	428	528	1.98±0.02	2.35	0.88	-1.47

4.2. Dye-sensitized titanium dioxide anodes

4.2.1. Structure of the photoanodes

The basic structure of the photoanodes consist in three parts. The base of the anodes is a transparent FTO coated glass which serves as support and charge transporter. The core of the anode is composed of TiO_2 which enables the water splitting reaction. The sensitive part is an organic dye which helps the system to take advantage of the visible sunlight to enhance its photoelectrochemical properties. Furthermore, we have added one more part, namely, rGO layer of different thicknesses to cover the system. It has the aim of protecting the dye from degradation and improve the electronic interchange between the system and the electrolyte, acting as a hole acceptor[26] (**Scheme 4**).

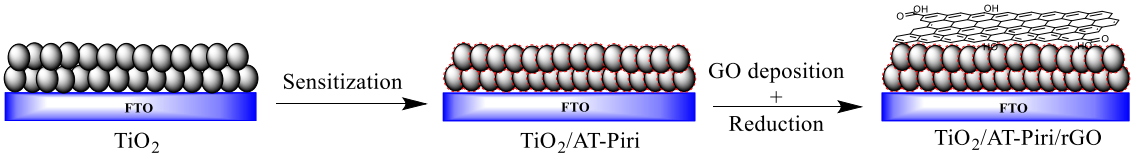

Scheme 4. Structure of the anode with the additions.

4.2.2. Characterization of the photoanodes

The characterization of the anodes was carried out by three techniques, which gives complementary information. The techniques were: Raman spectroscopy, ATR and SEM. The Raman spectroscopy was used to know how the anodes change in terms of phase composition and the relative quantities of the components. The ATR was followed with the aim to clarify the interaction between the TiO_2 and the dye and the SEM to give visual information about the surfaces.

Raman spectra for the different types of anodes are showed in **Figure 8**. There are two types of signals generated by the TiO_2. On the one hand the most intense at 140 cm^{-1} and, on the other hand, the three signals that appear at 400, 500 and 642 cm^{-1} which correspond to the anatase phase TiO_2, as they are the only signals present in the TiO_2 spectrum. In the TiO_2/AT-Piri spectrum there exist more signals, one around 1000 cm^{-1} and two peaks at 1457 and 1616 cm^{-1}. In the spectrums TiO_2/GO and TiO_2/rGO appear two bands around 1350 and 1600 cm^{-1}, which are commonly known as D band and G band respectively. The difference between them is in the D band as in the sample with

rGO the peak is higher than in the sample with GO. It is due to the restoration of the sp^2 carbons by the removal of oxygen moieties[27] and suggests that the reduction process was satisfactory. In the samples with rGO and AT-Piri there is an additional signal between the D and G bands, it can be a consequence of the interaction between the rGO and the dye. The last three of spectra correspond with anodes with the structure TiO_2/At-Piri/rGO x layers. It is clearly seen than with more rGO layers the intensity of the signals around 1500 cm^{-1} increases. It indicates that the amount of rGO deposited in each sample has also increased as it was expected.

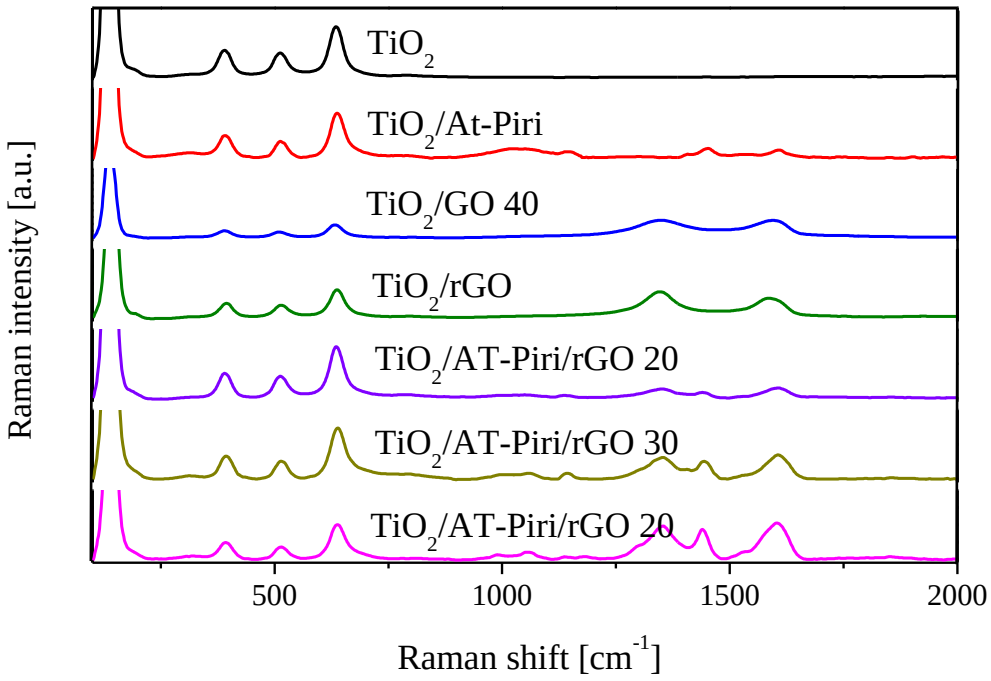

Figure 8. Raman spectra of the anodes.

Fourier transform infrared spectroscopy (FTIR) in transmission is the material characterization tool dedicated to the structural examination of adsorption modes at the anchor/substrate interface. Unfortunately, conventional transmission-based FTIR has yielded poor signal-to-noise ratios. Hence, attenuated total reflection (ATR-FTIR) is used instead. The capabilities of ATR-FTIR allow the wave to propagate along the region near the dye/ TiO_2 interface, which enhances the anchor-specific signal[19]. This technique has been used to assess the anchoring site of the dye in the TiO_2.The resulting spectra of both, the dye powder and the adsorbed on $TiO_2$are showed in **Figure 9**. The powder spectrum shows the characteristic stretching bands for C=N which is observed at around 1575 and 1428 cm^{-1}. However, in the spectrum of the dye adsorbed on TiO_2

an increase of the bands was observed at around 1601 and 1449 cm^{-1} that can be attributed to the nitrogen of the pyrimidine ring coordinated to the Lewis acid sites of the TiO_2 surface (Ti^{n+} cations) as it was reported in the literature with the analogous nitrogen atom of pyridine[28, 29, 30, 31].

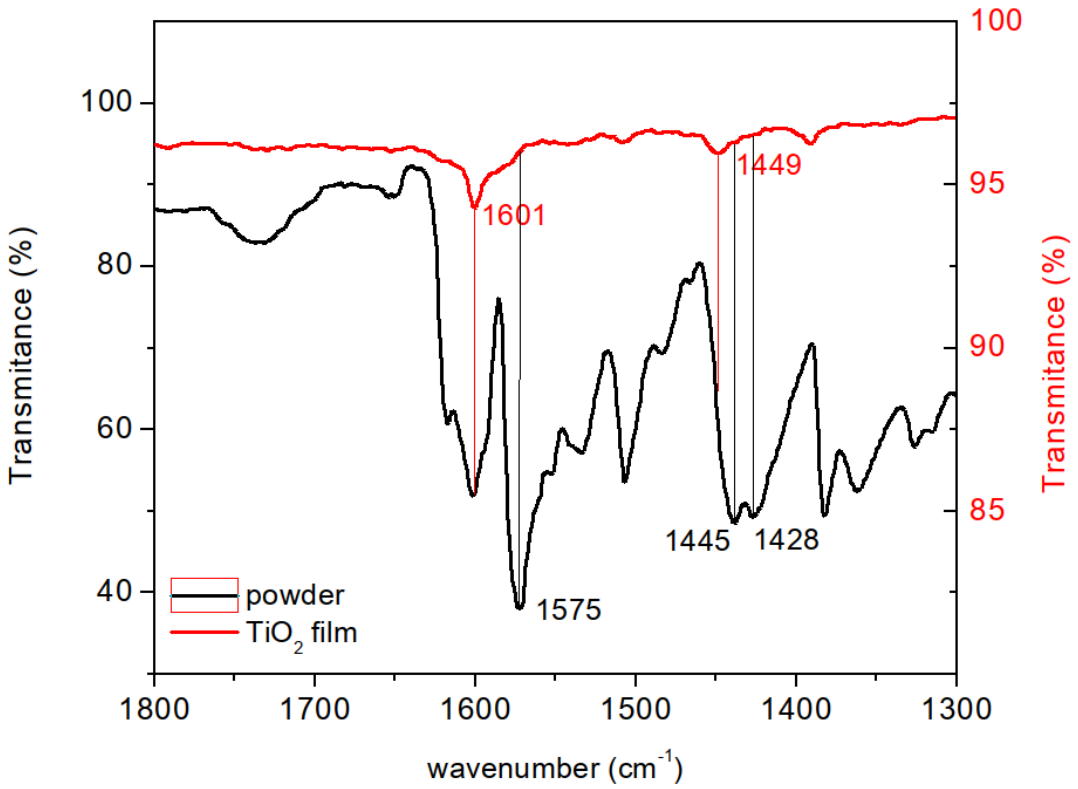

Figure 9. ATR-FTIR spectra of the dyes AT-Piri adsorbed on TiO_2 (red line) and powder (black line).

The SEM images are presented in **Figure 10**. Comparing the images of TiO_2 and TiO_2/AT-Piri there are not significant differences, since the dye attaches without changing the structure of the titanium oxide. Looking at the images in the right side, it can be seen the surface change when GO is added, as well as when it is reduced. In the images of the left side, there is a change in the roughness between the samples.

TiO_2

x10000 x12000

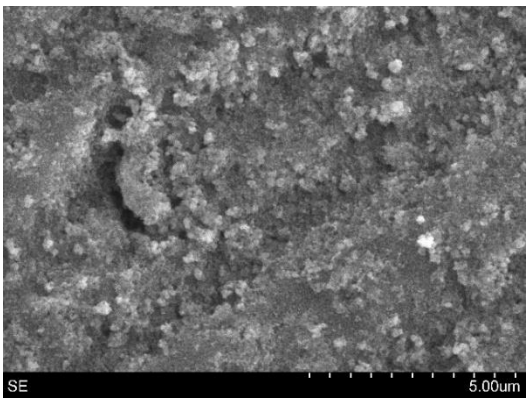

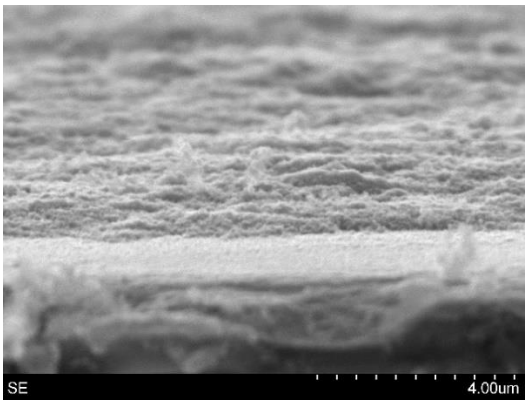

TiO_2/AT-Piri

x1500 x2100

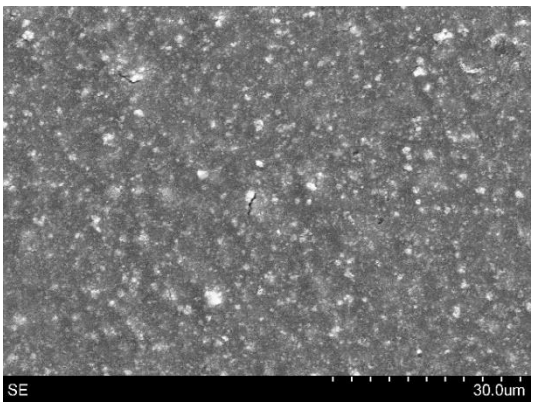

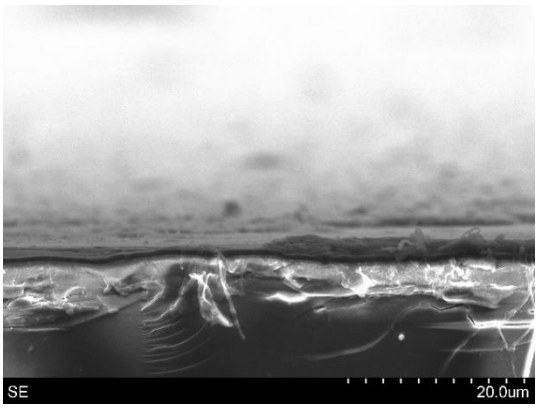

TiO_2/GO 40 layers

x1500 x5000

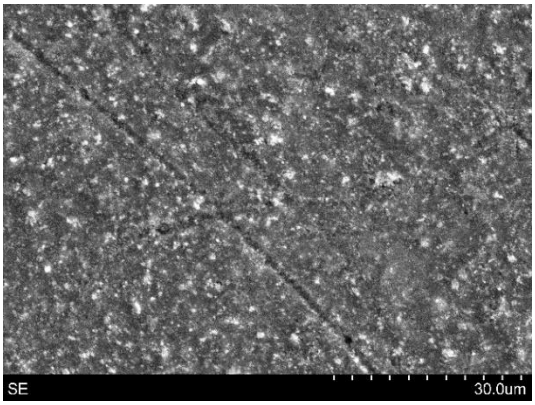

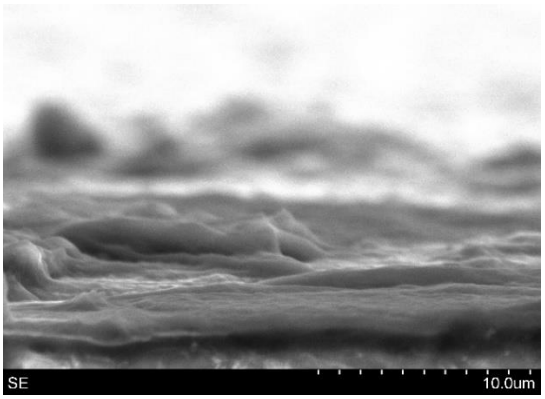

TiO_2/rGO 40 layers

x1500 x6000

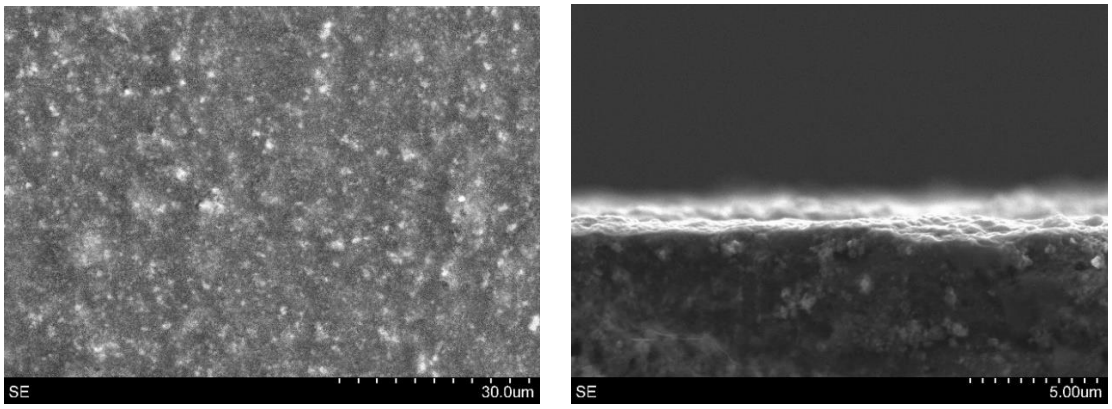

Figure 10. SEM images of anodes with different structures.

4.3. Photoelectrochemical behaviour

This section presents the photoelectrochemical study done to the anode and its variations. Initially, the effect of the application of several reductive cycles on the photoactivity of the system will be discussed. Then, the main study is presented, where the photoelectrochemical capabilities of six different anodes are followed.

4.3.1. Enhancement of the properties by the reduction of the system

In the first set of experiments, a correlation between the number of cycles done and the photocurrent was observed. To probe it, we designed an experiment in which 3 successive voltametric cycles were applied under irradiation. The sample used was a pristine anode with the structure TiO_2/AT-Piri. In the **Figure 11** the tendency is clear, the photocurrent rises while the anode is exposed to voltametric cycles. Despite the fact that the TiO_2 needs a reductive cycle to be activated, the behaviour exposed here cannot be explained by it. Looking at **Figure 11,** there exists a redox reaction in the system that increases the photocurrent produced while is stabilized with the cycles. This reaction is happening because of the dye, as it is not observed in the anodes with only TiO_2. This experiment remarks the necessity of make some previous reduction cycles to maximize the photocurrent produced in the following experiments.

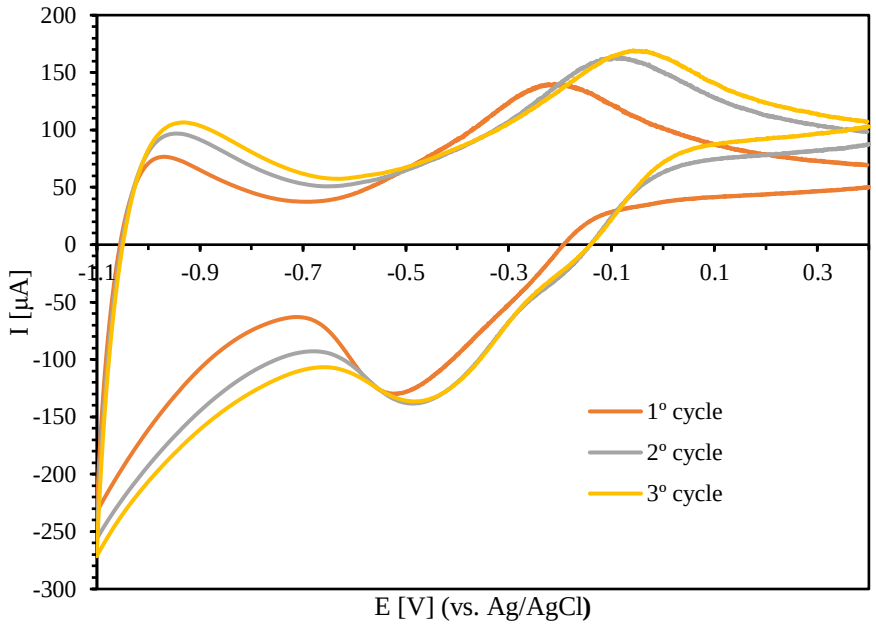

Figure 11. Cyclic Voltammograms of the anode TiO_2/AT-Piri.

4.3.2. Study in neutral pH medium

For this study, 6 different groups of anodes were prepared. Each group includes three identical anodes. Afterwards the labels are indicated:

1. TiO_2 → 1.1, 1.2, 1.3
2. TiO_2/AT-Piri → 2.1, 2.2, 2.3
3. TiO_2/rGO 40 layers → 3.1, 3.2, 3.3
4. TiO_2/AT-Piri/rGO 40 layers → 4.1, 4.2, 4.3
5. TiO_2/AT-Piri/rGO 20 layers → 5.1, 5.2, 5.3
6. TiO_2/AT-Piri/rGO 30 layers → 6.1, 6.2, 6.3

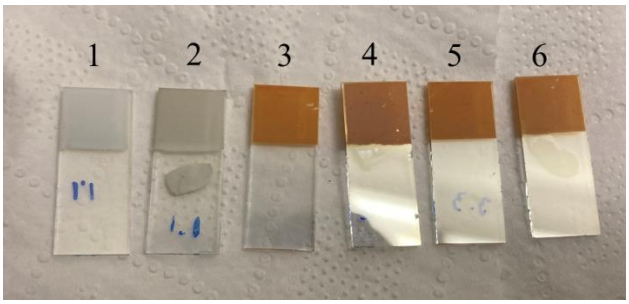

Figure 12. Type of anodes (1-6). The samples with GO (2, 4, 5, and 6) were not yet reduced.

A sequence of three experiments were done to each electrode. The sequence and the type of experiment were:

4.3.2.1. Four reduction cycles in darkness

This experiment consists in four successive reduction cycles carried out to stabilize the electrochemical properties and enhance the photocurrent produced, as was explained in 4.3.1. Additionally, it serves to reduce the GO into rGO in the series 3, 4, 5, and 6. It is done in darkness with the aim of preserving the anode photoactivity as high as possible.

As an example, **Figure 13** shows the reduction of the anode TiO_2/At-Piri/rGO 40 layers (4.1). In the voltammogram we see that upon the cycles the system tends to stabilize until the fourth one. The first one is the wider because of the GO reduction. Visually, it is possible to appreciate that rGO is darker than GO, which means that the reduction has happened, as it is showed in **Figure 14**.

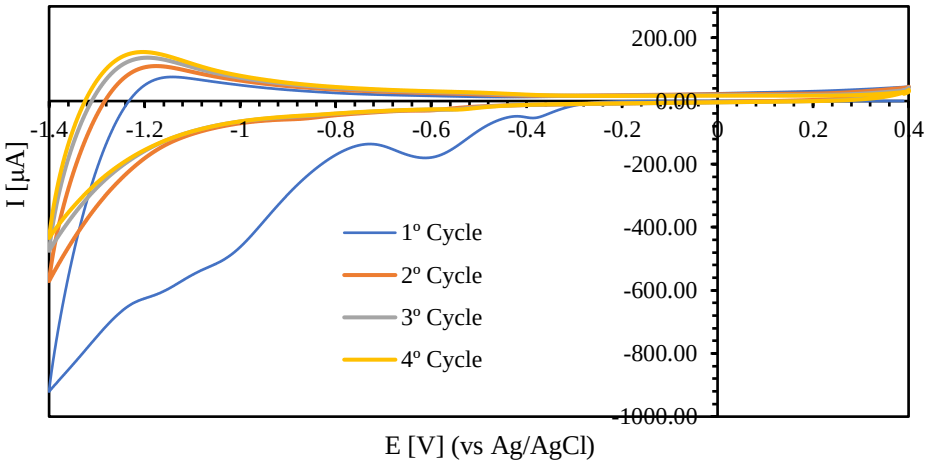

Figure 13. Cyclic voltammograms of anodes TiO_2/AT-Piri/rGO 40 layers in darkness.

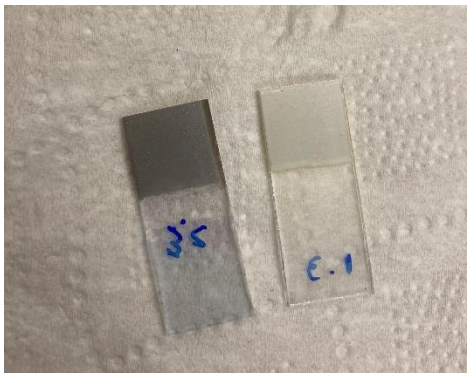

Figure 14. Anodes TiO_2/rGO (left) and TiO_2/GO (right).

4.3.2.2. Potentiostatic measurements

This experiment consists in keeping the voltage at 0 V (vs. Ag/AgCl) during 10 min. It was done under intermittent illumination. It provides information about the photocurrent produced by the anode along the time, as well as its transient behaviour. Between all the potentiostatic measurements done to all the electrodes, we have chosen the best one of each group (**Figure 15**).

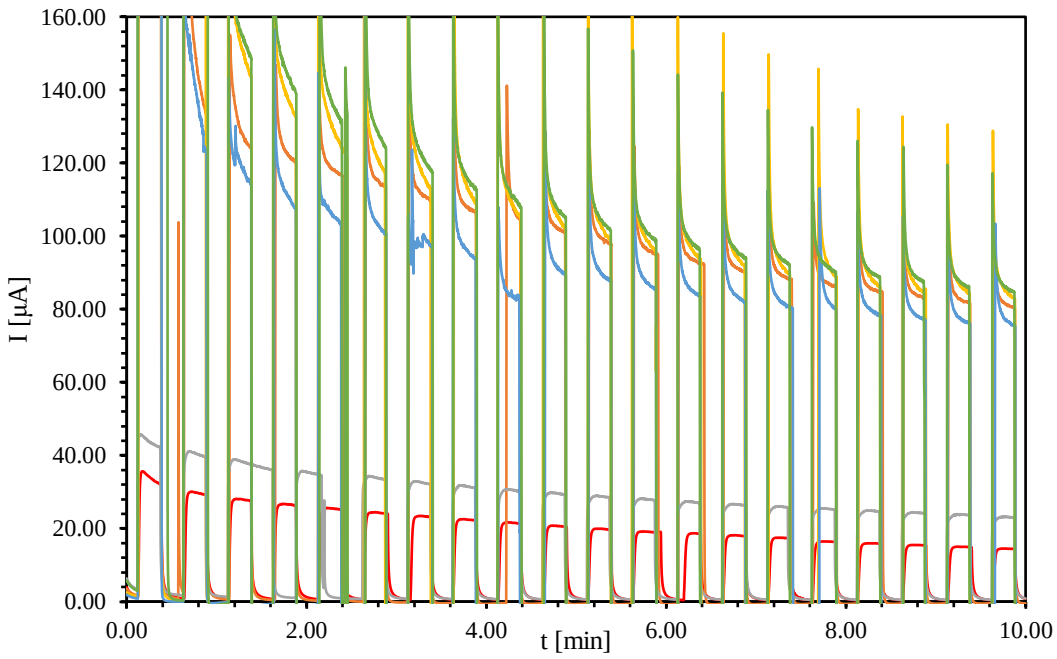

Figure 15. Photocurrent measurements of the six anodes: TiO_2, TiO_2/AT-Piri, TiO_2/rGO 40 layers, TiO_2/AT-Piri/rGO 40 layers, TiO_2/AT-Piri/rGO 20 layers, TiO_2/AT-Piri/rGO 30 layers.

The first conclusion to be drawn from the graph is the increase in the photocurrent produced by the sensitization of the TiO_2 with AT-Piri. The dye helps the anode to take more advantage of the sunlight spectrum, providing a larger number of holes to the TiO_2, which would increase the quantity of water that can be oxidated and, hence, the photocurrent produced. The sensitized anode with the dye AT-Piri produced around four times more photocurrent (80.38 μA) than the TiO_2 anode (22.86 μA), which is a huge improvement and underlines the potential of this type of electrodes.

Regarding the system TiO_2/rGO it is clear that the addition of the rGO increases the electrochemical capacities of the anode, acting as an efficient hole acceptor. As the addition of different rGO thicknesses on the surface of the anode is concerned, the one with 20 layers decreases the photoactivity of the system, while the others with 30 and 40 layers increase slightly. This photoactivity means that the performance of the TiO_2/AT-Piri anode can be tuned by the addition of some coatings with an adequate thickness.

4.3.2.3. Cyclic voltammetry (CV) measurements under illumination

The objective with these experiments is analogous to the described in the potentiostatic section 4.3.2.2.: to evaluate the photocurrent produced by the anode, but in this case with variable potential -1.4 to 0.4. Additionally, it is used to check the state of the anodes after the previous measurements.

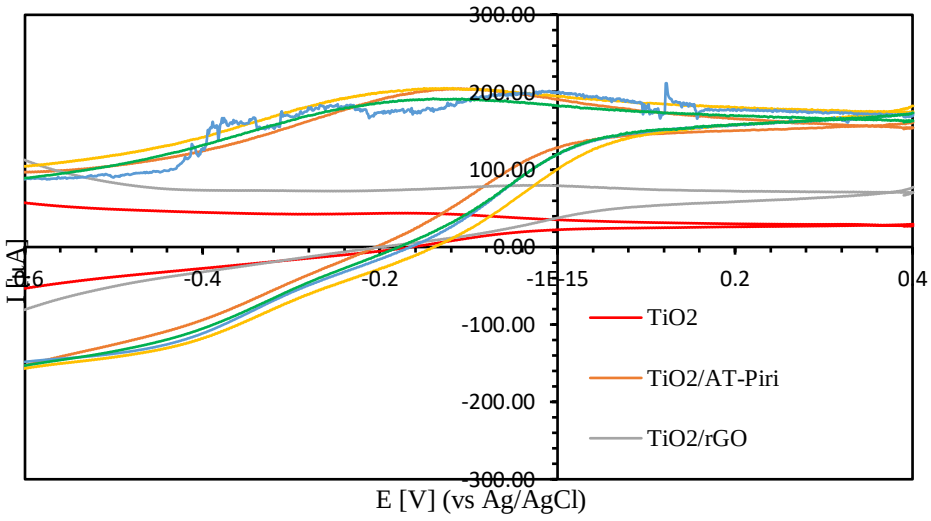

Figure 16. Cyclic voltammograms of the six anodes chosen the best one of each group.

Figure 16 depicts the cyclic voltammograms of the six anodes and the results barely differ from the potentiostatic ones. In this case the anode with 20 layers produces more photocurrent that the TiO_2/AT-Piri system. The difference is not remarkable enough, as the standard deviation in each series is around the same magnitude (**Table 2**).

Table 2. Photocurrent measurements (μA).

TiO_2			TiO_2/AT-Piri		
Sample	Potentiostatic	CV	Sample	Potentiostatic	CV
1.1	23	32	2.1	57	129
1.2	17	27	2.2	69	151
1.3	15	N.A.	2.3	80	152
Average	19	29	Average	69	144
Std. dev.	4	3	Std. dev.	11	13
TiO_2/rGO			TiO_2/AT-Piri/rGO 40 layers		
Sample	Potentiostatic	CV	Sample	Potentiostatic	CV
3.1	28	48	4.1	70	141
3.2	23	40	4.2	83	165
3.3	23	40	4.3	80	169
Average	24	43	Average	78	158
Std. dev.	3	5	Std. dev.	7	15
TiO_2/AT-Piri/rGO 20 layers			TiO_2/AT-Piri/rGO 30 layers		
Sample	Potentiostatic	CV	Sample	Potentiostatic	CV
5.1	57	130	6.1	67	133
5.2	77	144	6.2	85	161
5.3	75	168	6.3	68	119
Average	70	147	Average	73	138
Std. dev.	11	19	Std. dev.	10	21

4.4. Dye-sensitized solar cells (DSSC)

The method of photoanode preparation studied in the previous section 4.3. has been used to build several DSSCs to check its viability. The structure of the DSSCs cells will be presented, followed by the photovoltaic study.

4.4.1. Structure of the solar cell

The external part of the cell is composed by two FTO substrate glasses which are used to enclose the other parts and transmit the electrons. The anode is constituted by an analogous reduced structure, TiO_2/AT-Piri, previously described by 4.3.1. The cathode is prepared with a thin transparent layer of platinum. The electrodes are connected by the I^-/I_3^- electrolyte which closes the circuit and restores the oxidized dye (**Scheme 5**).

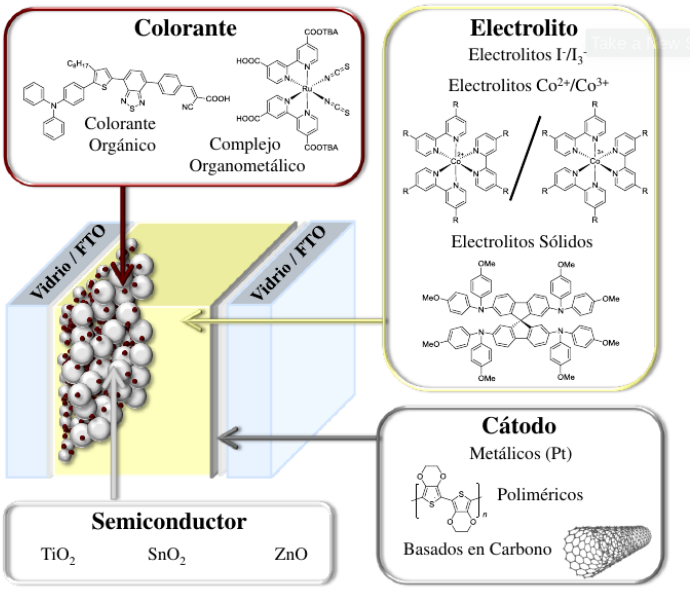

Scheme 5. Diagram of a DSSC[32].

4.4.2. Photovoltaic studies

This study has been carried out with two analogues DSSCs. These cells have been named as 1-TiO_2/AT-Piri and 2-TiO_2/AT-Piri, which in the following will be referred as 1 and 2, respectively. The *J-V* and the IPCE curves for the cell 2 are presented in **Figure 17**.

a) **b)**

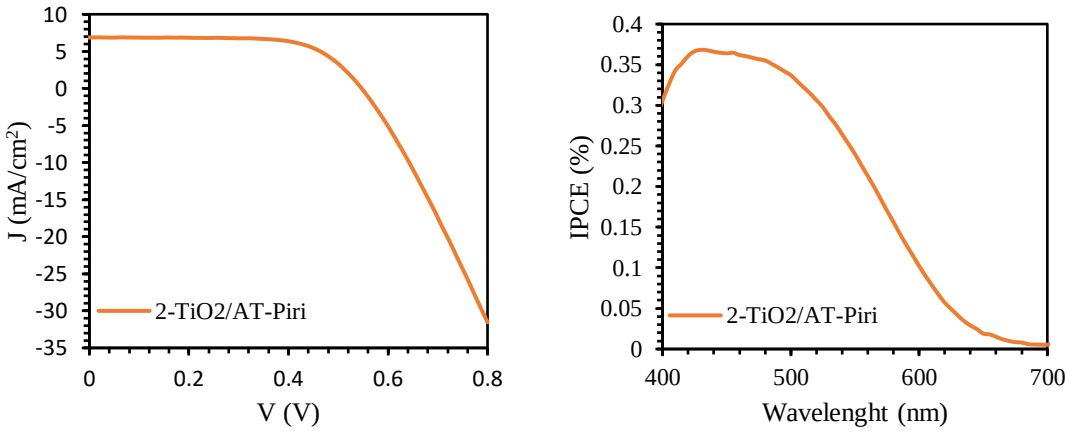

Figure 17. **a)** *J-V* curves of the DSSC 2. **b)** IPCE of the DSSC 2.

The novelty of this study was the active part of the cells 1 and 2 which was reduced by cyclic voltammetry, **Table 3**. The procedure is described in section 4.3.2.1., consisting

in four reduction cycles in darkness. Previously, our group did the same study using similar cells as 1 and 2 but without the reducing treatment (V_{oc} = 0.575 V; J_{sc} = 10.1 mA/cm^2; *FF* = 61.4 %; η = 3.87 %). A lower open circuit voltage and photocurrent parameters than the cell without the reducing treatment were obtained, which means that the reduction process does not favour the properties of the DSSC system.

Table 3. Parameters obtained from the *J-V* curves.

DSSC	V_{oc} (V)	J_{sc} (mA/cm^2)	*FF* (%)	*Efficiency* (%)
1-TiO_2/AT-Piri	0.50	5.82	52	1.50
2-TiO_2/AT-Piri	0.56	6.87	66	2.56

5. Conclusions

The photoanode TiO_2/AT-Piri is an adequate system for the water splitting. The photocurrent is four times higher with the sensitization of the TiO_2 by AT-Piri.

Reduction process has a positive influence on the novel photoanodes, related only with the water splitting process. Four reduction cycles were done to TiO_2/AT-Piri anodes and they improved the generation of photocurrent considerably.

The coating of the whole system with different thicknesses of rGO slightly increases the electrochemical capacity of the system by acting as an efficient hole acceptor.

The number of layers added has an influence and its quantity has to be modulated in order to obtain the best possible results.

6. Future work

This project has opened a wide range of possibilities in the field of water splitting, not only in terms of check different dyes, but also to find a good coating that can help the system in improving its characteristics.

7. References

1. Blakenmore, J.; Crabtree, R. H.; Brudvig, G. W. *Chem. Rev.* **2015**, *115*, 12974.

2. Ye, S.; Ding, C.; Liu, M.; Wang, A.; Huang, Q.; Li, C. *Adv. Mater.* **2019**, 31, 1902069.

3. Zhang, B.; Sun, L. *Chem. Soc. Rev*. **2019**, *48*, 2216.

4. McKone, J. R.; Lewis, N. S.; Gray, H. B. *Chem. Mater.* **2014**, 26, 407.

5. Bosserez, T.; Ronge, J.; van Humbeeck, J.; Haussener, S.; Martens, J. *Oil & Gas Scien. Tech.* **2015**, *70*, 877.

6. Fujishima A.; Honda K.*Nature*, **1972**, 238, 37.

7. Nakata, K.; Fujishima, A. *J. Photochem. Rev.* **2012**, 13, 169.

8. Abe, K.; Hara, K.; Sayama, K.; Arakawa, H.*J. Photochem and Photobio. A: Chem*, 137, **2000**, 63.

9. Agbe, H.; Nyankson, E.; Raza, N.; Dodoo-Arhim, D.; Chauhan, A.; Osei, G.; Kumar, V.; Kim, K. *J. Ind. Eng. Chem.* 72, **2019**, 31.

10. Choi, W. Y.; Termin, A.; Hoffmann, M. R. J. Phys. Chem. **1994**, 98, 13669.

11. Chen, X.; Glans, P. A.; Qiu, X.; Dayal, S.; Jennings, W. D.; Smith, K. E.; Burda, C.; Guo, J. *J. Electron Spectrosc. Relat. Phenom.* **2008**, *162*, 67.

12. Hagfeldt, A.; Boschloo, G.; Sun, L.; Kloo, L.; Pettersson, H. *Chem. Rev.*, **2010**, 110, 6595.

13. Zhang. S.; Yang, X.; Numata, Y.; Han, L. Energy Environ. Sci. 2013, 6, 1443.

14. O'Regan, B.; Grätzel, M. *Nature*, **1991**, *353*, 737.

15. Hirano, K.; Suzuki, E.; Ishikawa, A.; Moroi, T.; Shiroishi, H.; Kaneko, M. *J. Photochem. Photobiol., A.* **2000**, *136*, 157.

16. Young, K. J.; Martini, L. A.; Milot, R. L.; Snoeberger III, R. C.; Batista, V. S.; Schmuttenmaer, C. A.; Crabtree, R. H.; Brudvug, G. W. *Coord. Chem. Rev.* 256, **2012**, 2503.

17. Chem, X.; Shen, S.; Guo, L.; Mao, S. S. *Chem. Rev.* **2010**, 110, 6503.

18. Maeda, K.; Eguchi, M.; Youngblood, W. J.; Mallouk, T. E. *Chem. Mater.* **2008**, *20*, 6770.

19. L. Zhang and J. M. Cole, *ACS Appl. Mater. Interfaces*, **2015**, 7, 3427.

20. Rousset, E.; Ciofini, I.; Marvaud V.; Hanan, G. S.; *Inorg. Chem.*, **2017**, 56, 9515.

21. Otsuka, H.; Kobayashi, A.; Yoshida, M.; Kato, M. *J. Photochem. Photobiol.*, A, **2019**, 369, 189.

22. Ooyama, Y.; Nagano, T.; Inoue, S.; Imae, I.; Komaguchi, K.; Ohshita, J.; Harima, Y. *Chem. Eur. J.*, **2011**, 17, 14837

23. Morita, K.; Takijiri, K.; Sakai, K.; Ozawa, H.; *Dalton Trans.*, **2017**, 46, 15181.

24. Costa, S. P. G.; Batista R. M. F.; Cardoso P.; Belsley M.; Raposo M. M. M. *Eur. J. Org. Chem.* **2006**, 17, 39.

25. Nüesch, F.; Grätzel, M. *Chem. Phys.* **1995**, 193. 1.

26. Hernández-Ferrer, J.; Ansón-Casaos, A.; Víctor-Román, S.; Sanahuja-Parejo, O.; Martínez, M. T.; Villacampa, B.; Benito, A. M.; Maser, W. K. *Electrochemica Acta*, 298, **2019**, 279.

27. Hidayah, N. M. S.; Liu, W.; Lai, C.; Noriman, N. Z.; Khe, C.; Hasmin, U.; Lee, H. C. Amer. Inst. Phys. Conf. Proc. 1892, 150002**, 2017**.

28. Ooyama, Y.; Nagano, T.; Inoue, S.; Imae, I.; Komaguchi, K.; Ohshita, J.; Harima, Y. *Chem. Eur. J.*, **2011**, 17, 14837.

29. Mohamed, M. M.; Bayoumy, W. A.; Khairy, M.; Moussa, M. A. *Microporous Mesoporous Mater.* **2007**, 103, 174.

30. Vishwanathan, V.; Roh, H.-S.; Kim, J.-W.; Jun, K.-W. *Catal. Lett.* **2004**, 96, 23

31. Zaki, M. I.; Hasan, M. A.; Al-Sagheer, F. A.; Pasupulety, L.; *Colloids Surf. A*, **2001**, 190, 261.

32. Diseño, síntesis y estudio de nuevos sistemas push-pull para su aplicación en dispositivos solares. Tesis: Raquel Pérez Tejada, **2015**.

Appendix

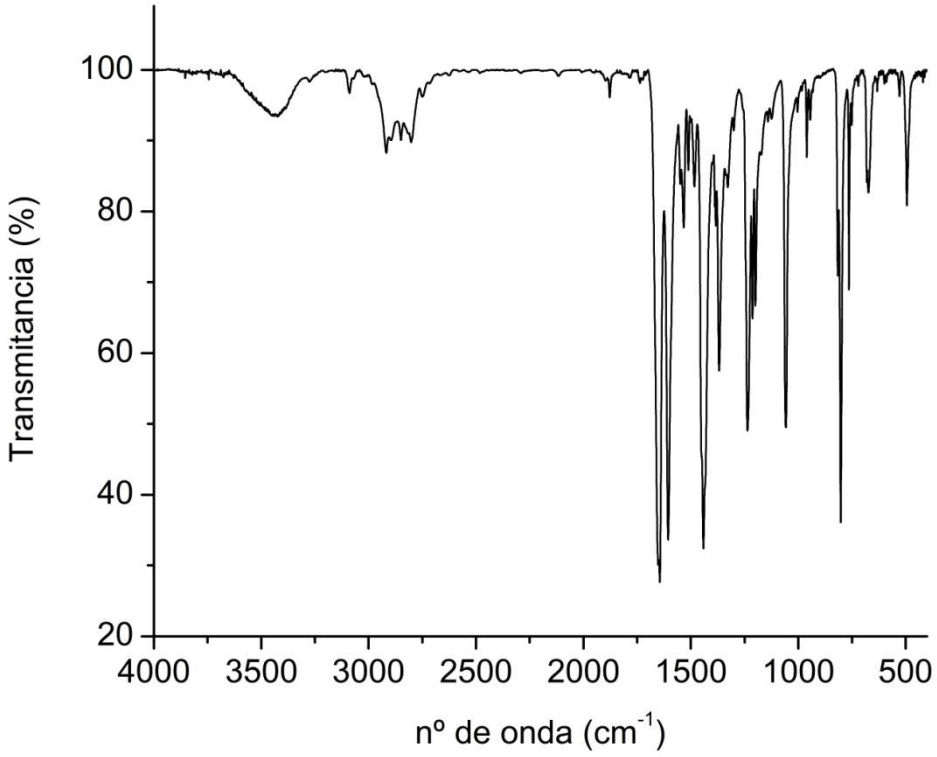

Figure A10. IR spectrum of precursor 1.

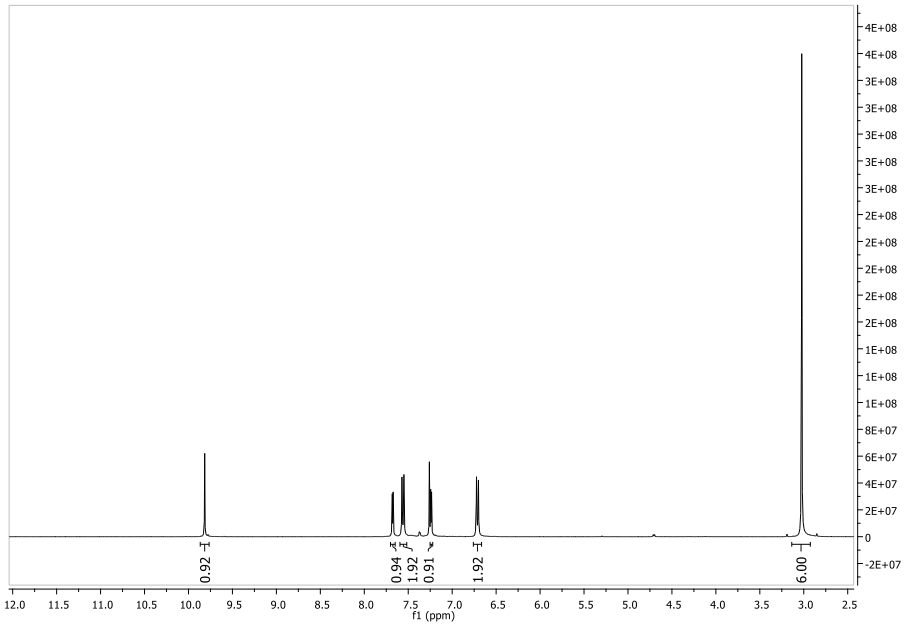

Figure A2. ^{1}H-RMN spectrum of precursor 1.

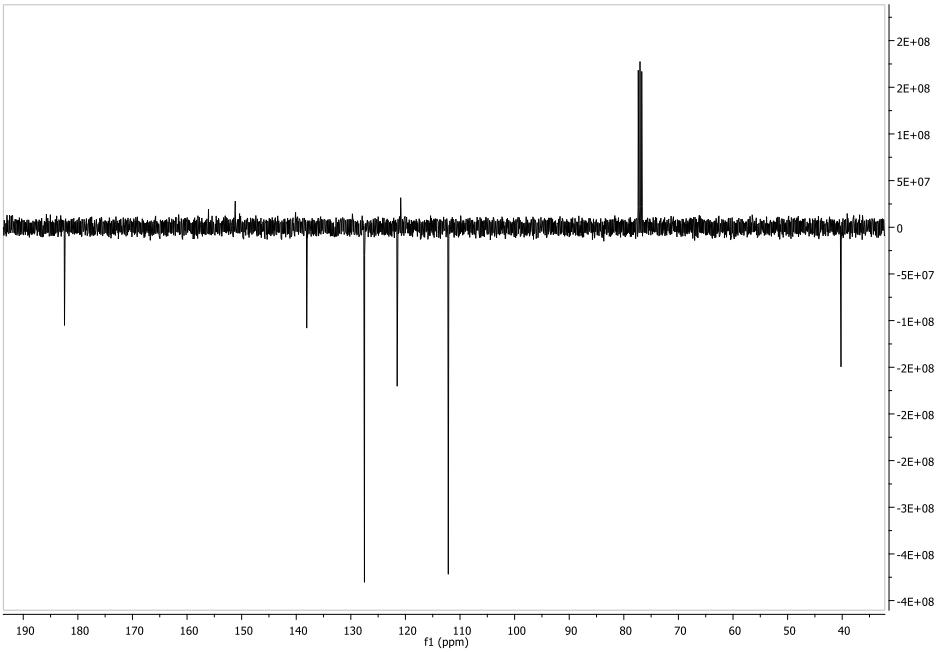

Figure A3. ^{13}C-RMN spectrum of precursor 1.

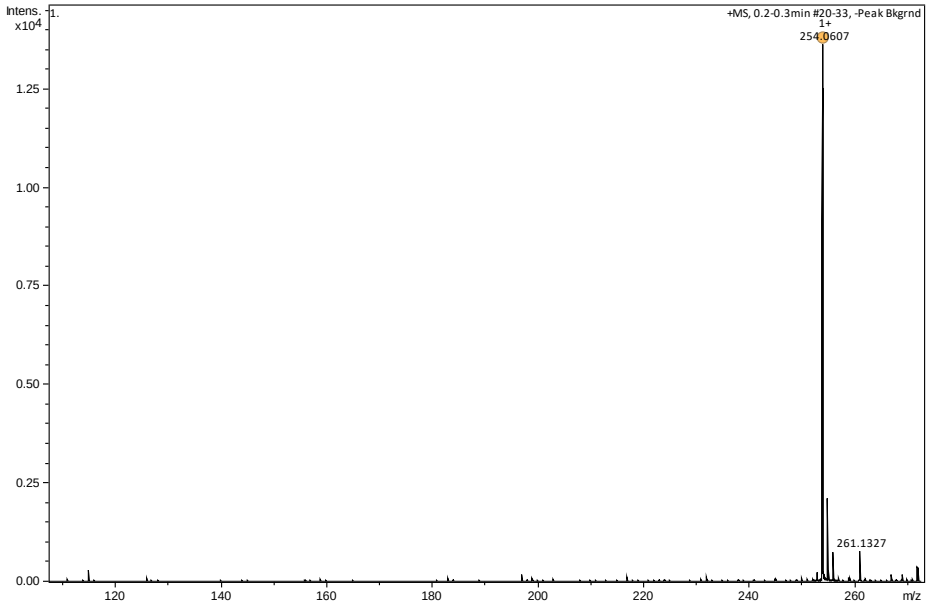

Figure A4. HRMS (ESI$^+$) spectrum of precursor 1.

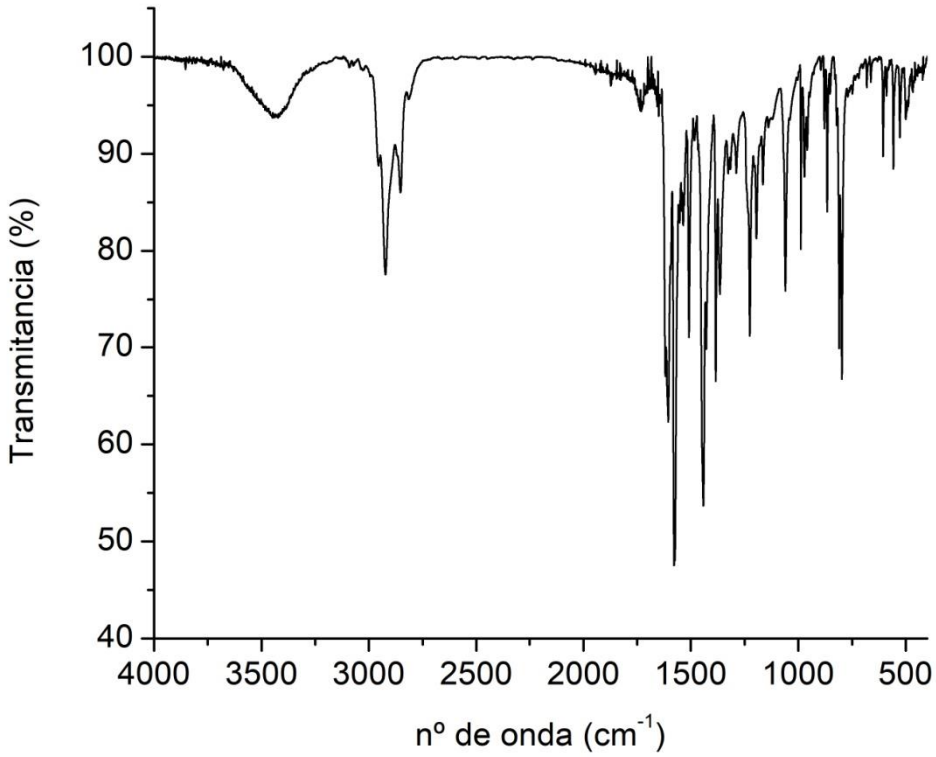

Figure A5. IR spectrum of **AT-Piri.**

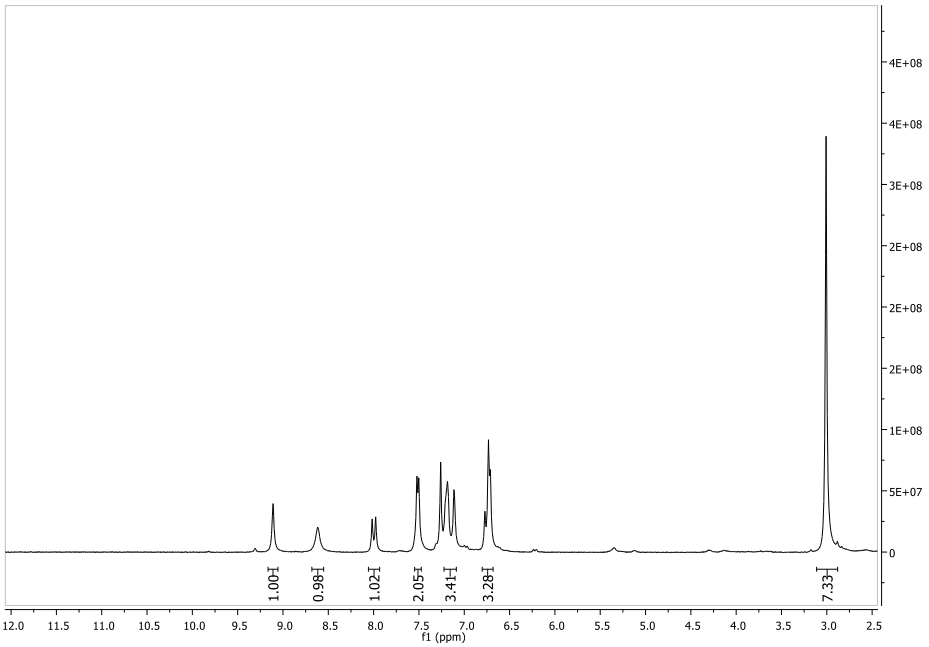

Figure A6. ^{1}H-NMR spectrum **AT-Piri** ($DCCl_3$).

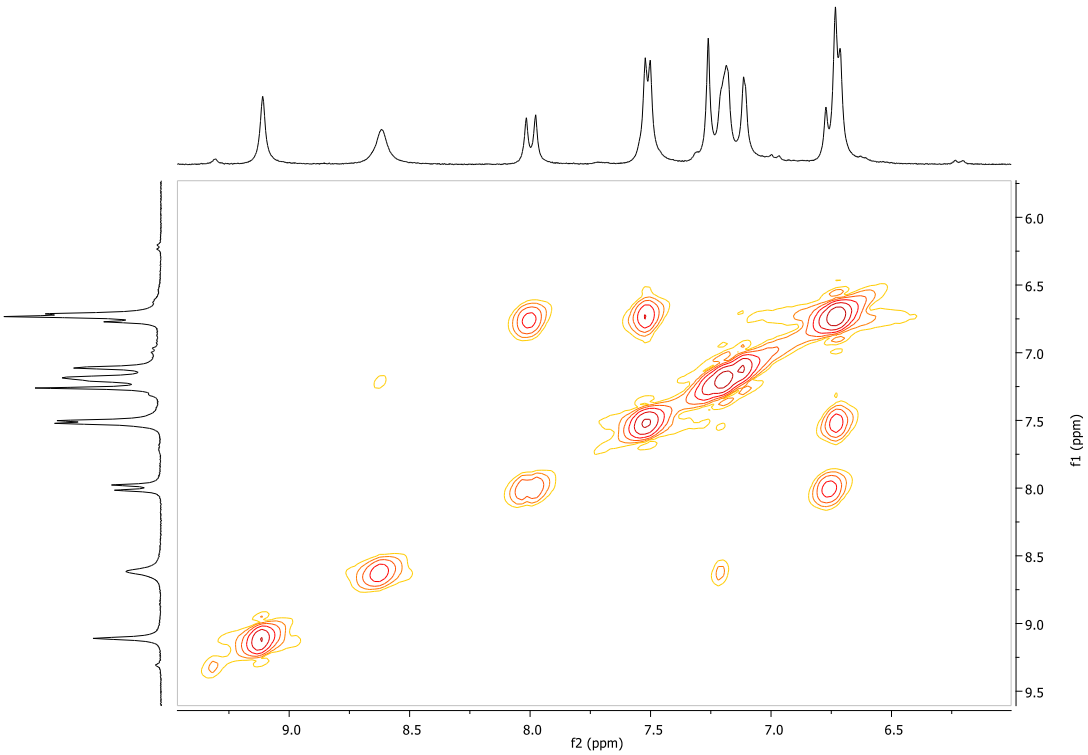

Figure A7. COSY ^{1}H-^{1}H spectrum **AT-Piri.**

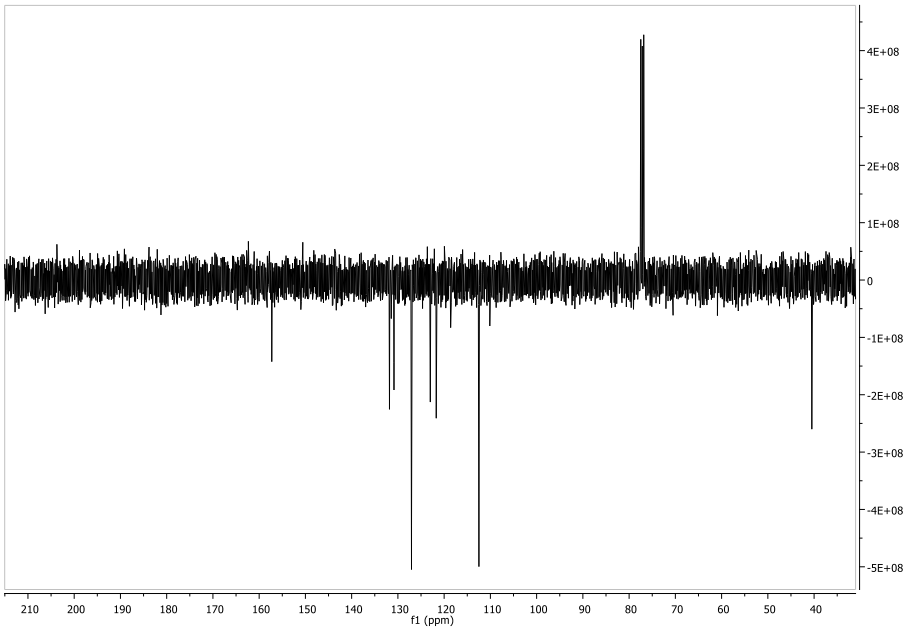

Figure A8. ^{13}C-NMR (APT) spectrum of **AT-Piri** ($CDCl_3$).

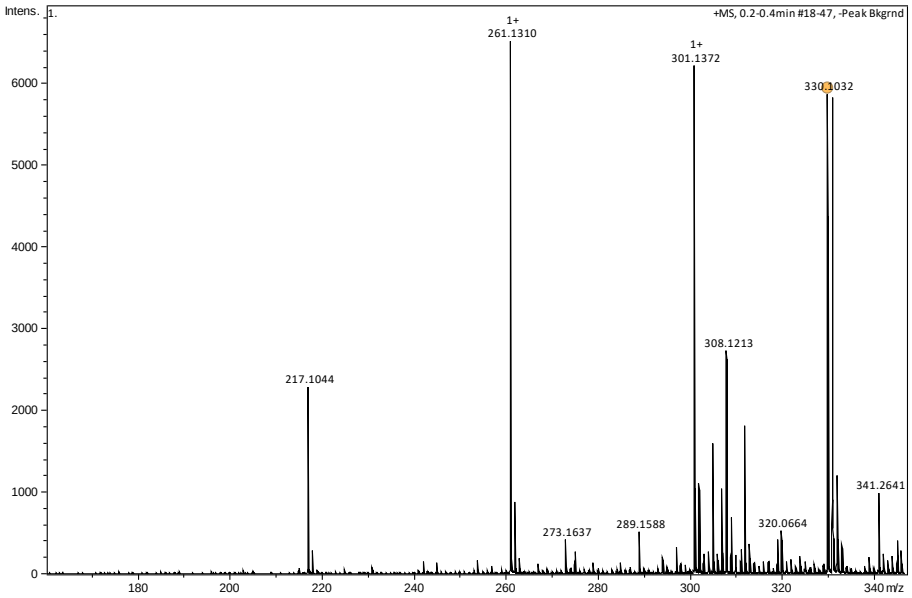

Figure A9. HRMS (ESI^+) spectrum of **AT-Piri.**

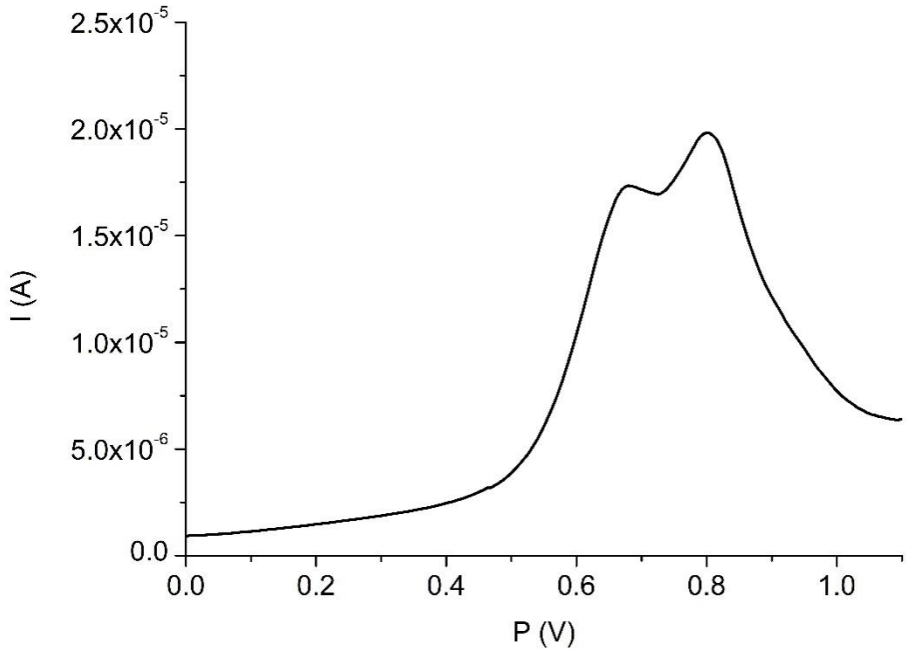

Figure A10. DPV measurement of **AT-Piri** (vs Ag/AgCl).

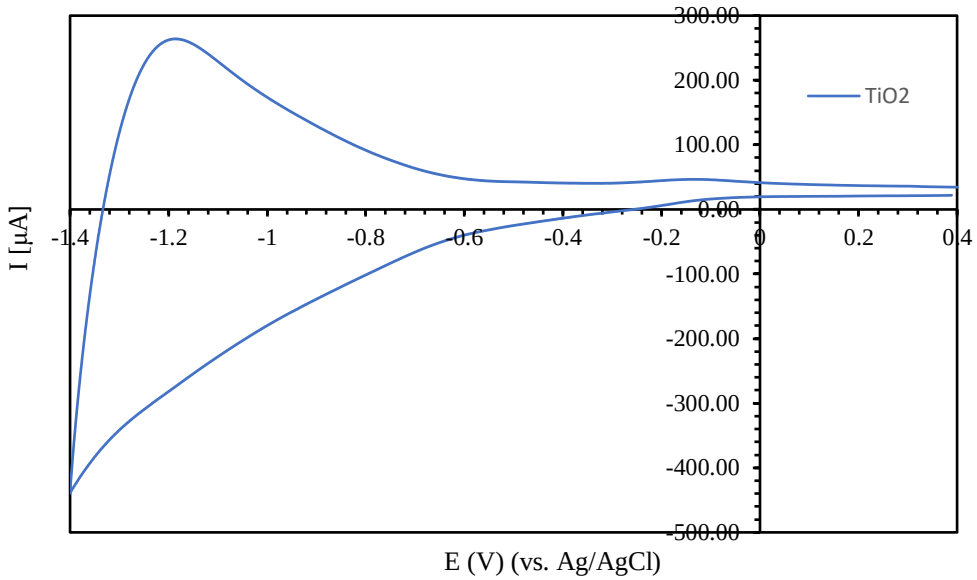

Figure A11. Voltammogram of TiO_2 under illumination.